Master's Thesis

Academic Year 2021

Numerical investigation on electrical and thermal characteristics in organic semiconductor films from the aspect of variable range hopping

Graduate School of Science and Technology,
School of Integrated Design Engineering,
Keio University

Descouens Nicolas

81923362

A Master's Thesis
submitted to Graduate School of Science and Technology, Keio University
in partial fulfillment of the requirements for the degree of
MASTER of School of Integrated Design Engineering

Descouens Nicolas

Advisor: Associate Professor Noda Kei

Abstract of Master's Thesis of Academic Year 2021

Numerical investigation on electrical and thermal characteristics in organic semiconductor films from the aspect of variable range hopping

Category: Science / Engineering

Summary

Keywords:

Graduate School of Integrated Design Engineering, Keio University

Descouens Nicolas

Acknowledgements

Table of Contents

List of Figures

Chapter 1
Introduction

1.1 Organic semiconductors

1.1.1 Background

For the past century, inorganic materials have been at the heart of the semiconductor industry, with element such as silicon, germanium or gallium arsenide. But, the industry turned itself to new devices and organics semiconductor are one of them. Their different set of properties: very flexible, low cost, less polluting helped them to gain interest.

More specifically, in 1977, the first highly conducting polymer was found, chemically doped polyacetylene, was discovered [7]. Such materials can be easily processed by techniques already know in the industry: vacuum evaporation, solution casting... But a better understanding and control of the self-assembly of molecules, as well as a booming research field, have increased greatly the performances, reaching the charge carrier mobility of amorphous silicon for some of them (fig. 1.1). The high diversity of geometry within the material allows a better tuning of the characteristic of the semiconductor to the use. One greater advance is the combination of both organic and inorganic molecules, particularly with perovskite. The high mobility of inorganic material combined with the more flexible geometry of organic ones make possible the creation of devices that reaches the performances of single-crystal silicon [18, 24].

This new development has been seen through the recent appearance of organic devices in the market. The more flagrant one is OLED devices, they offer a better diversity (flexible screens) with increased performance (higher color fidelity, darker black and better contrast) as well as consumption. But it's also used in professional devices such as OTFT [17], laser diode [22], ...

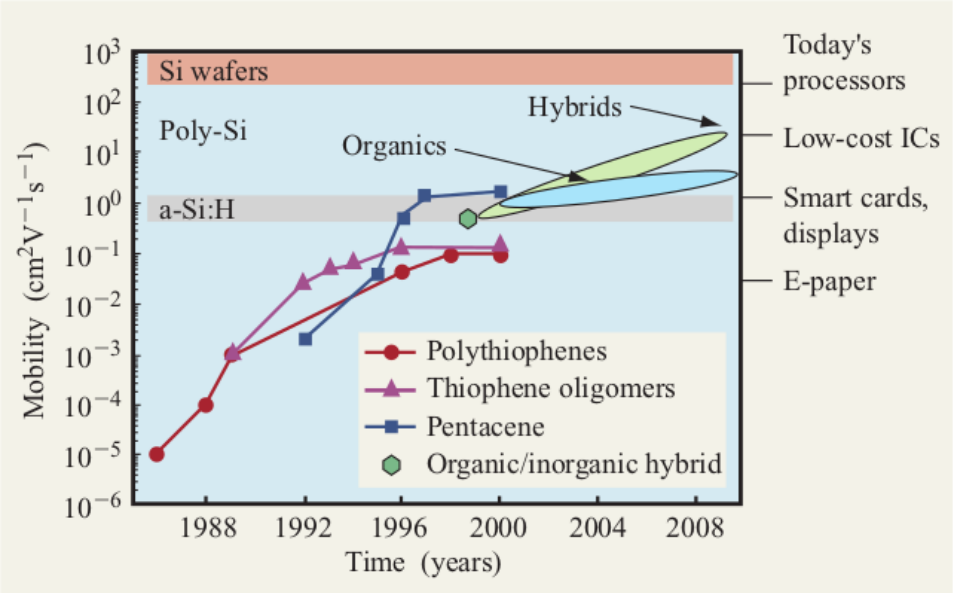

Figure 1.1: Evolution of the performance for some organic semiconductors [24]

1.1.2 Organic materials

Organic molecule are bound to each other by $\pi - \pi$ bounding which are the result of p_z-orbitals of sp^2-hybridized C-atoms in the molecules (fig. 1.2). Such bonding is way weaker compared to the classic σ-bounding in the molecule backbone. Therefore, the $\pi - \pi^*$ transitions have a typical lower gap: around 1.5 eV$-$3 eV (fig. 1.3). Their crystallinity ranges from single-crystal (pentacene, rubrene crystals) [30] to completely amorphous semiconductors like α-NPD [27].

Those weaker Van der Waals bonding lead to more localized charge carrier in the material. Most of the time, charge carriers do not evolve in bands like in Si, but are subject to a HOMO (Highest Occupied Molecular Orbital) and LUMO (Lowest Unoccupied Molecular Orbital) states. It results in a much weaker wavefunction delocalization for the neighboring molecules [5]. Instead of band transport, organic materials are subject to hopping transport: a charge carrier hop from a site to an other and thus participate to the general conduction (fig.1.4). The difference between trapping and hopping state is in the recombination and release rate. if the former one is higher than the letter one, the state is a recombination center, otherwise, it is a trap. In this model the difference between trapping states and recombination states can be thin.

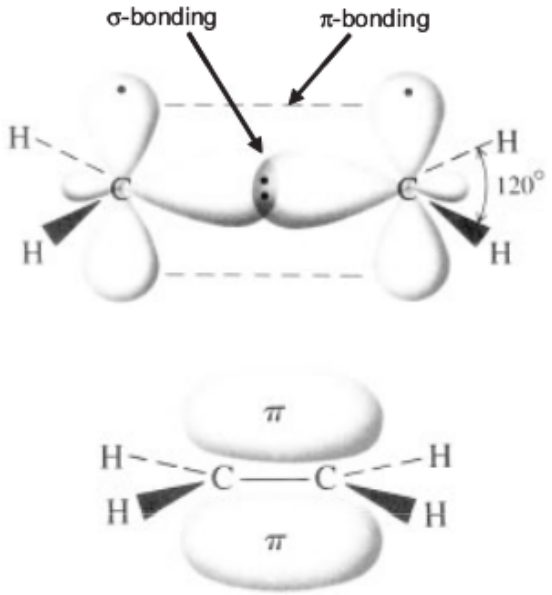

Figure 1.2: σ and π bonds in ethene [5]

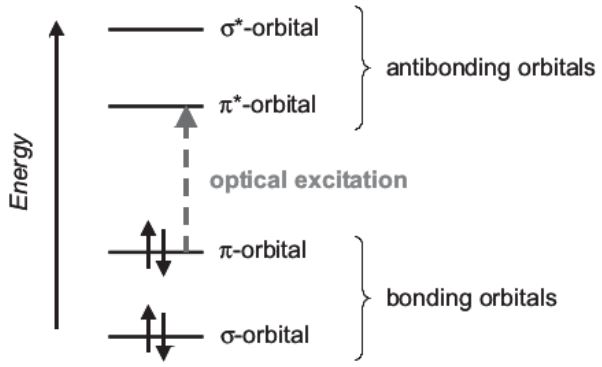

Figure 1.3: $\pi - \pi^*$ bonding [5]

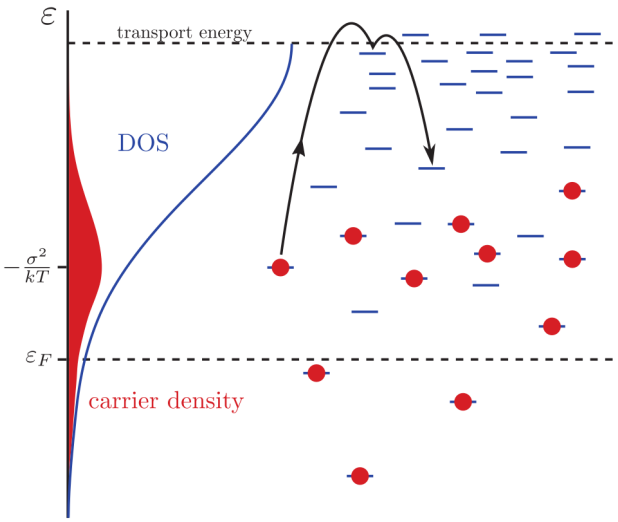

Figure 1.4: Hopping transport

Organic semiconductors are divided between polymers and small molecules. The separation occurs at 1000 molecular weights. Small molecules can achieve high cristallinty but are less soluble in solvent, requiring dry processes such as vacuum deposit, which is more difficult and more costly. On the other hand, polymer are easier to made in organic solvents. Even though small molecules show better performances, they're less stable than polymer in atmospheric conditions.

1.1.3 Charge carrier transport

As it has been said before, disorganized organic semiconductors are the place of localized charge carrier transport, and in the 70's, a theory has been proposed involving tunneling between near states [1]. Such theory as been previously discovered by Mott based on the dependence of the mobility on the temperature: an increasing temperature leads to an increasing mobility. This relation has been verified in practical devices [1, 13].

In the variable range hopping theory (VRH), the displacement between two states for a charge carrier is determined only by the difference in energy W and in position R, thus highlighting the fact that our system is resolutely in 4D. On top of that, we assume that the system is so disordered that this two quantities are decoupled. The jump frequency is usually described by the Miller-Abrahams formalism [16]:

$$\nu = \nu_0 \begin{cases} \exp\left(-2\alpha R_{ij} - \frac{E_j - E_i}{k_B T}\right) : E_j - E_i \geq 0 \\ \exp\left(-2\alpha R_{ij}\right) : E_j - E_i \leq 0 \end{cases} \tag{1.1}$$

- ν_0: base-jump frequency
- R_{ij}: distance between initial state i and final state j
- α: decay constant of the assumed hydrogen-like localized state wave functions
- E_i: energy of the state i

Depending on the position of the final state j, the formula change. If the state is on higher energy, it requires tunneling to occur on the energetic part, whereas if the reaching state if of a lower energy, only the distance is taken into account for the tunneling effect.

Using this formalism, it is possible to access the mobility and diffusivity for charge carrier.

1.1.4 The einstein relation

Classical einstein relation

$$\frac{D}{\mu} = \frac{k_b T}{q} \tag{1.2}$$

- μ: mobility
- D: diffusion
- k_B: Boltzmann constant
- T: temperature
- q: elementary charge

The einstein relation [8], is a useful equation that link two quantities, μ and D over a simple equation. D constitutes a key parameter in analyzing semiconductor but is not so easy to measure. On the contrary, the mobility is easily accessed. However, in the presence of energetic disorder, such simple equation does not seem to hold [3, 20]. In non-equelibrium cases, it also seems that we can't use this relation anymore, the relation between the diffusion and the field seems to be quadratic [19].

Generalized equation

From the limit of the eq. 1.2, a new relation has been proposed, taking into account the dependence on the carrier concentration [21]:

$$\frac{D}{\mu} = \frac{n}{q\partial n/\partial E_F} \tag{1.3}$$

- E_F: quasi-Fermi level
- n: carrier concentration

With n being the carrier concentration defined by the fermi-dirac distribution $f = \frac{1}{1+exp\left(\frac{E-E_F}{k_BT}\right)}$ and g the gaussian density of state [21]:

$$n = \int_{-\infty}^{\infty} \frac{g(E)}{1 + \exp\left(\frac{E-E_F}{k_BT}\right)} dE \tag{1.4}$$

Such eq. 1.4 has been calculated following the hypothesis that drift and diffusion of charge carrier at fermi level are exactly compensated, meaning that there is no net current and is only valid for low electric field.

From this stating, a more suitable equation has been proposed in the following thesis.

1.1.5 Gaussian density of states

$$g(E) = \frac{N}{\sigma\sqrt{2\pi}} \exp\left(-\frac{E^2}{2\sigma^2}\right) \tag{1.5}$$

Gaussian density of states has been suggested by numerous monte-carlo simuations [6] as well by the observation of the excitonic absorption profile which is gaussian too. Besides, the intrinsic localization behavior of the gaussian density of state fit very well the observation made on real devices.

From a mathematical point of view, the disorder is directly linked to σ, which broadens the bell-shaped of the function (fig. 1.5, 1.6).

1.1.6 Thermal diffusion

Organic semiconductors have recently received much attention regarding their potential thermoelectric effect. From their figure of merit (eq. 1.6)

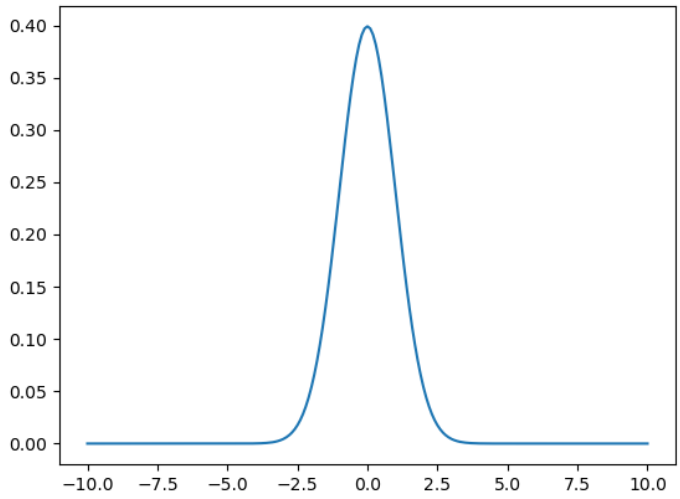

Figure 1.5: Gaussian DOS, $\sigma = 1$

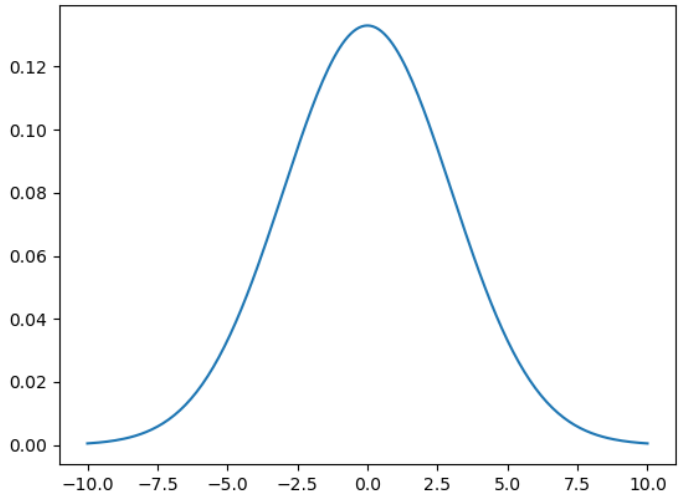

Figure 1.6: Gaussian DOS, $\sigma = 3$

$$\mathrm{ZT} = \frac{\sigma \cdot S^2}{\kappa} T \tag{1.6}$$

- S: Seebeck coefficient
- σ: electrical conductivity
- κ: thermal conductivity

From ZT value is representative of the electric efficiency of the device. Thus a lower thermal conductivity κ naturally leads to higher figure of merit and to an increased energetic conversion.

A better understanding of the process is key to engineering better devices, but the classical theory used on inorganic material [9] can't be applied directly to organic ones. The variety of morphology in organic semiconductors plays a great role in defining its thermal characteristics and is extremely sensitive to the spacial arrangement of the molecules within the material.

To simulate the thermal effect, one should take into account both charge carrier and phonon transport: $\kappa = \kappa_e + \kappa_p$ with a slight predominance of the phonon in the process of thermal conduction [14].

1.2 Objectives of this thesis

The overall understanding of both electric and thermal behavior of organic semiconductors is scarce. Their great diversity, which is at the heart of their recent success, makes it difficult to get an simulation of the charge carrier in the material. The goal of this thesis is to obtain, thanks to equations developed throughout the 20th century and to new hypothesis on the comportment of the charge carrier, as well as a powerful computer language, a reasonable approximation of the electric and thermal figures in doped organic semiconductors. Our objectives are:

- Estimate einstein ratio for many type of organic semiconductors
- Estimate the thermal conduction by taking into account both charge carrier and phonon participation
- Take into account the doping behavior of the semiconductor, as well as the disorder and electric effect

- Simulate the behavior in a fairly small amount of time

The novelty of this study resides in the multitude of the parameters taken into account and in new behavior for charge carrier within the material.

Chapter 2
Electric properties

The framework for the electric properties, diffusion, mobility and einstein ratio will be detailed in this section. As now on, we will adopt the following formalism. If not stated otherwise, every quantity written in lowercase will be reduced and all the quantity in uppercase will be the non-reduced equivalent (u_F is the reduced quantity of U_F). To reduce the unit we will use respectively for the energetic dimension and spatial dimension:

$$\begin{aligned} u &= \frac{U}{k_b T} \\ r &= 2\alpha R \end{aligned} \tag{2.1}$$

k_B being the Boltzmann constant and $\alpha = 4.34 \times 10^7\,\mathrm{cm}^{-1}$ the decay constant of the assumed hydrogen-like localized state wave functions.

2.1 Gaussian formalism

To simulate the localized behavior of charge carrier, we will use a gaussian density of states (gaussian DOS) for doped semiconductor. The doping effect will take form of an another gaussian with a different peak. The origin of the energy will be taken to be the LUMO level, but this theory works for holes and electron alike: an energy inversion is will bring us into the hole formalism.

$$\begin{aligned} g\left(E, \hbar\omega_\alpha\right) = &\frac{1}{\sqrt{2\pi}} \left\{ \frac{N_{i-e}}{\sigma_i} \exp\left(-\frac{\left(E - \hbar\omega_\alpha\right)^2}{2\sigma_i^2} \right) \right. \\ &\left. + \frac{N_{d-e}}{\sigma_d} \exp\left(-\frac{\left(E - \hbar\omega_\alpha + E_d\right)^2}{2\sigma_d^2} \right) \right\} \end{aligned} \tag{2.2}$$

- $N_{i-e}(cm^{-3})$: density of charge carriers for the intrinsic material

- $N_{d-e}(cm^{-3})$: density of charge carriers for the doped material
- $\hbar\omega_\alpha(J)$: mode effect, vibration of the lattice
- $\sigma_i(J)$: width of the intrinsic gaussian, representative of the disorder of the intrinsic material
- $\sigma_d(J)$: width of the doped gaussian, representative of the disorder of the doped material
- $E_D(J)$: energy shift between intrinsic and doped material

g_e is expressed in $cm^{-3}J^{-1}$.

On the figure 2.1, the doping results in a broadening of the DOS, which is coherent with doping increasing the number of states within the material.

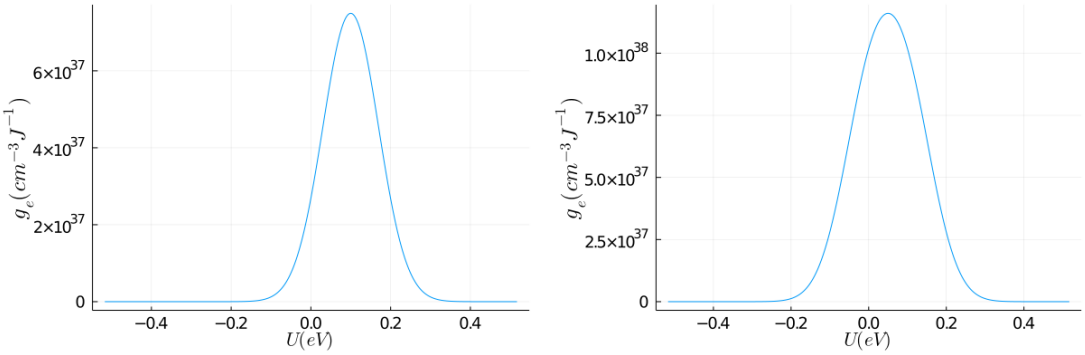

(a) Non-doped semiconductor

(b) Doped semiconductor
$N_{d-e} = 2.1 \times 10^{18}\,\mathrm{cm}^{-3}$, $E_D = 0.1\,\mathrm{eV}$

Figure 2.1: DOS doping comparison
$T = 300K$, $N_{i-e} = 2.1 \times 10^{18}\,\mathrm{cm}^{-3}$, $\hbar\omega_\alpha = 0.16 \times 10^{-19}\,\mathrm{J}$

Using the Fermi-Dirac distribution, the carrier concentration is:

$$n = \int_{-\infty}^{+\infty} \frac{g_e(U)}{1 + exp\left(\left(\frac{U-(\hbar\omega_\alpha+U_F)}{k_B T}\right)\right.} dU \tag{2.3}$$

2.2 Variable range hopping

2.2.1 Background

We suppose that the charge carrier jump by tunneling from one state to another. The system is thus described in 4 dimensions: 3 for the spatial dimension, and one for the energy.

In our semi-classical model, we define the average probability for a jump to be the geometrical mean for all the jump within a material:

$$\langle P \rangle = \lim_{n\to\infty} \left[\prod_i^n P_i \right]^{1/n} = \exp \left[\lim_{n\to\infty} \frac{1}{n} \sum_i^n \ln P_i \right] \tag{2.4}$$

P_i being a singular jump in the material, we make the average over all the jump in the material.

As the arithmetic mean is more familiar, it's easier to work with the $\frac{1}{n}\sum_i^n \ln P_i$ part. To do so, we define the distance hopped to be:

$$r_i = -ln(P_i) \tag{2.5}$$

The i arises from the fact that $P_i < 1$ and the logarithm is thus negative. Finally, we get:

$$\langle P \rangle = exp(-r_{nn}) \tag{2.6}$$

With r_{nn} being the mean range to the nearest neighbor for each state throughout the material. This theory making the average over all the states in the material has the advantage of summarizing the spatial and energy distribution of the states in on variable r_{nn}. The Miller-Abrahams hopping rate can now be written as:

$$\nu = \nu_0 \cdot exp(-r_{nn}) \tag{2.7}$$

Usually, ν_0 which is the basic hopping rate is set to 1×10^{13} Hz.

If we define P_{ij} to be the probability of a jump from the state i to the state j, from an energetic standpoint:

$$P_{ij}^{energy} = exp\left(\frac{U_i - U_j}{k_B T}\right) = exp(u_i - u_j) \tag{2.8}$$

From a spatial standpoint:

$$P_{ij}^{spatial} = exp\left(-2\alpha L_{ij}\right) = exp(-l_{ij}) \tag{2.9}$$

We can fairly assume that:

$$P_{ij} = P_{ij}^{total} = P_{ij}^{energy} \cdot P_{ij}^{spatial} = e^{[u_i - u_j] - l_{ij}} = e^{r_{ij}} \tag{2.10}$$

We write the field effect as: $\beta = \frac{Fe}{2\alpha k_B T}$, F being the field intensity in Vcm^{-1}. Of course, the course of a charge carrier is modified by the field. To model this, we include it directly in the equation of the 4D distance: a state alongside the field direction will be seen as closer or father depending on the angle θ between R_{ij} and F:

$$\left.\begin{array}{ll} R_{ij} & = (1 + \beta\cos\theta)L_{ij} + (U_j - U_i) \quad \text{for } U_j > U_i - \beta\cos\theta R_{ij} \\ & = L_{ij} \qquad\qquad\qquad\qquad\quad \text{for } U_j < U_i - \beta\cos\theta R_{ij} \end{array}\right\} \tag{2.11}$$

$(1 + \beta\cos\theta)$ arises from the shift of the fermi level due to the field (fig. 2.2). We assume here that for states to lower energy, only the physical distance is taken into account as the charge carrier does not need to make a jump to higher energies.

2.2.2 Nearest neighbor

The quantity r_{nn} can be computed thanks to the formula of the "number of free states" $\mathscr{N}$, the mean number of free state at a distance $\mathscr{R}$ [1] of a state. We suppose that the material is disorganized enough to make both energetic and spatial dimension uncorrelated, and that the states are equally distributed in respect of the gaussian DOS.

$$\mathcal{N}\left(u, T, \beta, \mathscr{R}\right) = \int_0^{\pi}\int_0^{\mathscr{R}}\int_{-\infty}^{\mathscr{R}+u-r(1+\beta\cos\theta)} g\left(v\right)\left[1 - F\left(v\right)\right]\frac{k_B T}{8\alpha^3} \times 2\pi r^2 \sin\theta dv dr d\theta \tag{2.12}$$

$g(1-F)$ represent the emptiness of a state, F being the Fermi-Dirac equation, $1-F$ is the probability of the state to be empty, i.e a state where a charge carrier can jump. $\frac{k_B T}{8\alpha^3}$ is simply a reducing factor to eliminate the unit of $g(1-F)$. $4\pi r^2$ is the surface of a sphere with a radius r and $\frac{1}{2}\sin\theta$ makes the average between the field effect direction and the direction of r. The $\frac{1}{2}$ factor arises from the integral $\int_0^{\pi}\frac{1}{2}\sin\theta = 1$. The born in the energetic integral $\mathscr{R} + u - r(1 + \beta\cos\theta)$ correspond

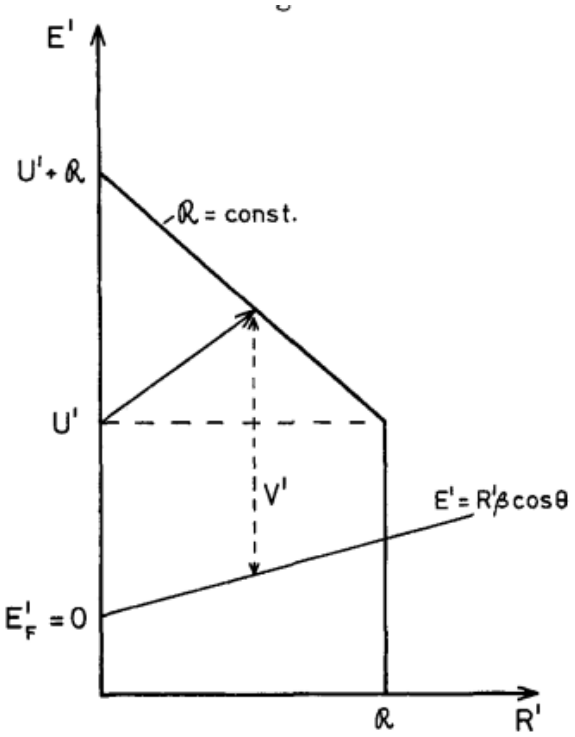

Figure 2.2: Energetic-spatial relationship (source [1])

to the maximum energetic value for a jump of distance $\mathscr{R}$. Finally, $\mathcal{N}$ computes the number of states enclosed enclosed in a 4D sphere of radius $\mathscr{R}$.

We thus define r_{nn} being the radius at which we found in average, 1 free state, i.e $\mathcal{N}(r_{nn}) = 1$.

This method for computing $\mathscr{N}$ is similar to the percolation criteria, but they take $\mathcal{N}(r_{nn}) = 2.8$, 2.8 being the percolation criteria. But, where the percolation theory intends to find a path of jump within the material, our r_{nn} quantity means the nearest free states, which intuitively corresponds to the distance at which we find 1 state.

From the figure 2.3, we see that for low value of energy, the quantity r_{nn} skyrockets. The rarefaction of available states due to the Fermi-Dirac distribution means that for a charge carrier to find an available spot is harder. On the opposite, we see a plateau at higher energetic values. At such energy, charge carrier can make energetically favorable jump to lower states, which depends only on the intrinsic characteristics of the material (the state distribution $g(1 - F)$). Mathematically, the born $\mathscr{R} + u - r(1 + \beta \cos\theta)$ makes it happen: for lower u,

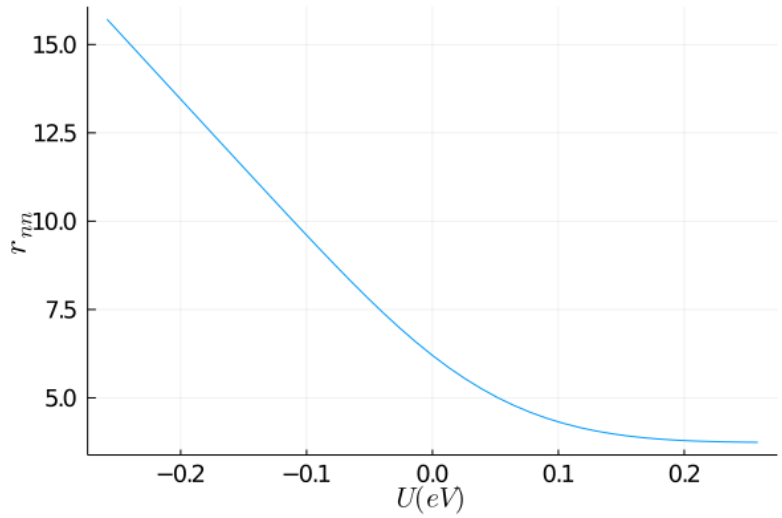

Figure 2.3: r_{nn} behavior for pentacene, $F = 5.3\,\mathrm{V\,cm^{-1}}$ (pentacene parameters appendix A)

$\mathscr{R}$ compensate to cover the spectrum $g(1-F)$, and for higher energy, u alone is enough to cover it.

2.2.3 Real hopped distance

With r_{nn}, we have an insight of the geometry of the material, but what really matters to find the diffusion or mobility is the average displacement of the charge carrier, that we will name x_F. Of course, such quantity is affected by the field intensity.

We first define:

$$
\begin{aligned}
I_1 &= \int_0^{\pi} \int_{u-r_{nn}\beta\cos\theta}^{u+r_{nn}} g(v)\,[1-F(v)] \left[\frac{r_{nn}-v+U'}{1+\beta\cos\theta}\right]^3 \sin\theta\cos\theta\, dv d\theta \\
I_2 &= \int_0^{\pi} \int_{-\infty}^{u-r_{nn}\beta\cos\theta} g(v)\,[1-F(v)]\, r_{nn}^3 \sin\theta\cos\theta\, dv d\theta \\
I_3 &= \int_0^{\pi} \int_{u-r_{nn}\beta\cos\theta}^{u+r_{nn}} g(v)\,[1-F(v)] \left[\frac{r_{nn}-v+U'}{1+\beta\cos\theta}\right]^2 \sin\theta\, dv d\theta \\
I_4 &= \int_0^{\pi} \int_{-\infty}^{u-r_{nn}\beta\cos\theta} g(v)\,[1-F(v)]\, {r_{nn}}^2 \sin\theta\, dv d\theta
\end{aligned}
\tag{2.13}
$$

And the distance written as:

$$x_F = \frac{I_1 + I_2}{I_3 + I_4} \tag{2.14}$$

The eq. 2.14 is a weighted mean. I_1 and I_3 represent jumps to state of higher energy, thus involving not only the distance but the energy. I_2 and I_4 represent jumps to state of lower energy, thus involving only the spatial distance hopped.

$\left[\frac{r_{nn}-v+U'}{1+\beta\cos\theta}\right]$ is comparable to a distance. If we take the expression $v = r_{nn} + u - r(1+\beta\cos\theta)$ from the eq. 2.12, we find for the distance r:

$$r = \left[\frac{r_{nn} - v + U'}{1+\beta\cos\theta}\right] \tag{2.15}$$

Moreover, to understand better the role of this integral, it is better to split it in two parts. First:

$$w = g(v)\left[1 - F(v)\right]\left[\frac{r_{nn} - v + U'}{1+\beta\cos\theta}\right]^2 \sin\theta dv \tag{2.16}$$

This is the weight and represent the number of state at a certain distance r.

The function $f(v) = \left[\frac{r_{nn}-v+U'}{1+\beta\cos\theta}\right]\cos\theta$ represents the distance to a free state pondered by the field effect $\cos\theta$.

Finally, we can sum up the relation 2.14 by:

$$x_F = \frac{\int_{V_1} f(v)w(v) + \int_{V_2} f(v)w(v)}{\int_{V_1} w(v) + \int_{V_2} w(v)} \tag{2.17}$$

With V_1 and V_2 being the surface of integration.

The energy dependency (fig. 2.4) see two plateaus, one a high energy is 0, meaning that at this level, most of the jump are made only downward in energy. For the negative energies, the depletion in free state due to the Fermi-Dirac distribution makes the jump to be of a higher distance. But it reaches a plateau because at a certain point, the jump is made in energy to reach near Fermi level states.

By looking a little bit more into detail on I_1 and I_2 (fig. 2.5, 2.5), we can justify mathematically the global behavior of x_F. I_2 is similar to a gaussian bell because $g(1-F)$ dominates the integral. However, for I_1, for positive values we have indeed the lower born of the integral that $u - r_{nn}\beta\cos\theta$ that goes beyond the high density zone of states. Concerning the lower values, the increase of r_{nn}

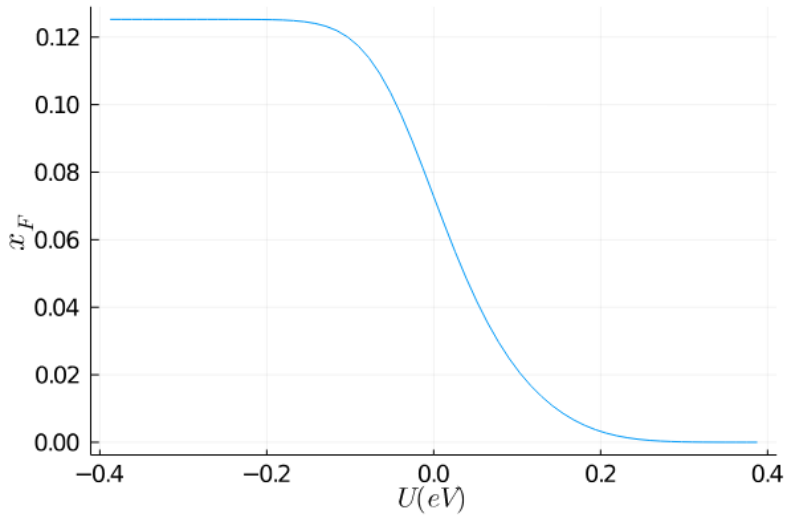

Figure 2.4: x_F dependence on energy, $F = 5.3\,\mathrm{V\,cm^{-1}}$ (pentacene parameters appendix A)

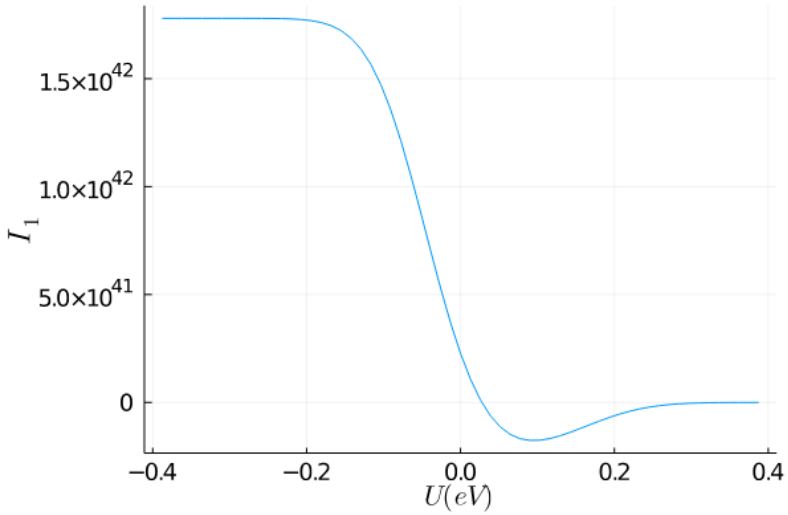

Figure 2.5: I_1 dependence on energy, $F = 5.3\,\mathrm{V\,cm^{-1}}$ (pentacene parameters appendix A)

compensate the decrease of energy u, making the upper limit $u + rnn$ more or less constant.

By studying the influence of the field on x_F (fig. 2.7), we see that it reaches a

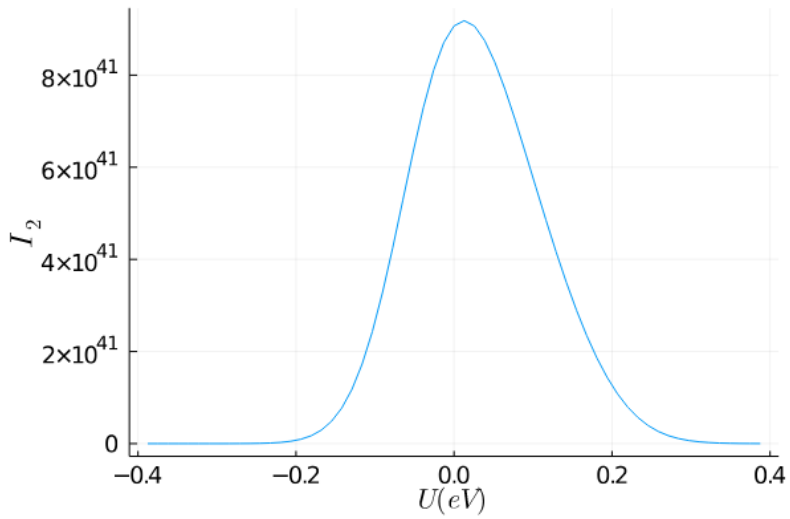

Figure 2.6: I_2 dependence on energy, $F = 5.3\,\mathrm{V\,cm^{-1}}$ (pentacene parameters appendix A)

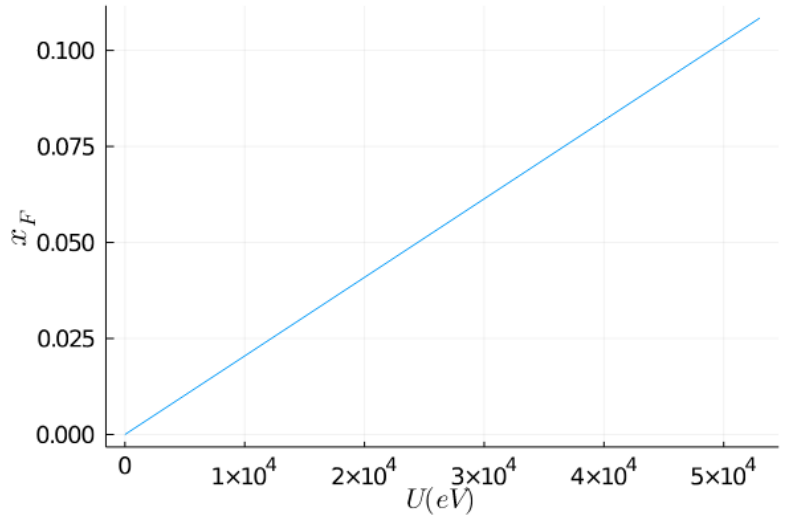

Figure 2.7: x_f dependence on the field, $F = 5.3\,\mathrm{V\,cm^{-1}}$ (pentacene parameters appendix A)

limit at which x_F decreases. Physically, the field increases so much that it starts extracting the charge carrier from the material. In top of that, $\lim_{x\to 0} xf = 0$. Indeed, if the charge carrier is not influenced by an electric field, its surrounding

his uniform regarding the angle θ, thus the jump are equidistant regarding all the direction.

2.2.4 Mobility

Mobility is classically defined as the average velocity of the particle divided by the force. In our case, the mean distance jumped being x_F and a particle jumps at a rate (eq. 2.7):

$$\mu = \frac{\langle x \rangle}{F} = \frac{\nu_0 X_F e^{-r_{nn}}}{F} \tag{2.18}$$

From the equation 2.18, we can plot the mobility depending on the energy (figure 2.8). At low energy, the charge carrier are globally trapped and can't participate to the mobility. However, at higher energy, we already noticed that the jump are made in great majority regarding the energy and not regarding spatial coordinates. Thus the mobility for higher value drops to 0.

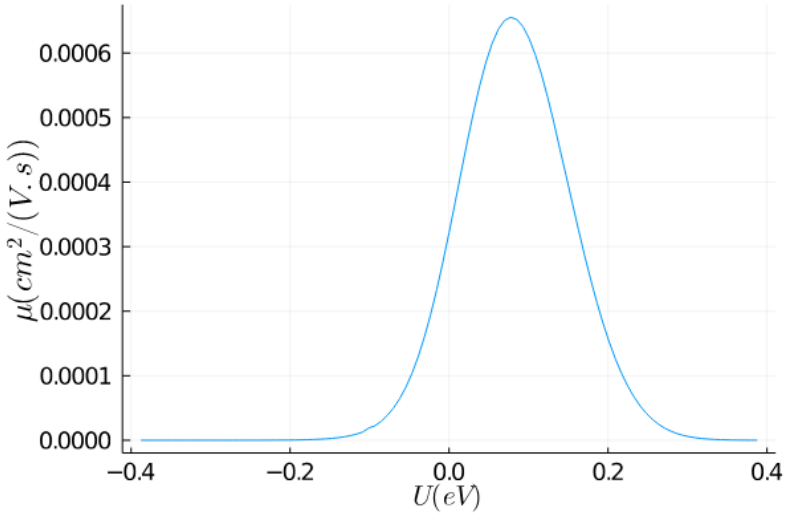

Figure 2.8: μ dependence on the energy, $F = 5.3\,\mathrm{V\,cm^{-1}}$ (pentacene parameters appendix A)

From the formula 2.18, we can compute the conductivity σ:

$$\sigma(U) = q g_e(U) F(U) \mu(U) k_B T \tag{2.19}$$

We see on the figure 2.9 that the curve is shifted toward LUMO level. The majority of the free charge carrier being situated near this level, it is natural for the conductivity to do the same.

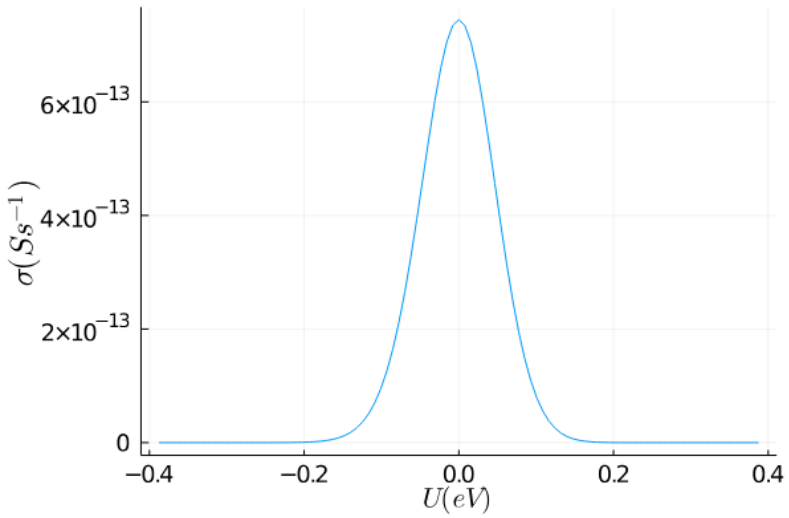

Figure 2.9: σ dependence on the energy, $F = 5.3\,\mathrm{V\,cm^{-1}}$ (pentacene parameters appendix A)

Of course the mobility is only defined for a sample affected by a field.

We define the global mobility in the material as $\mu(u)$ weighted by the number of states:

$$\mu = \frac{\int_{-\infty}^{+\infty} \mu(u)g(u)F(u)du}{\int_{-\infty}^{+\infty} g(u)F(u)du} \tag{2.20}$$

In a similar way, we define:

$$\sigma = \frac{\int_{-\infty}^{+\infty} \sigma(u)g(u)F(u)du}{\int_{-\infty}^{+\infty} g(u)F(u)du} \tag{2.21}$$

2.2.5 Stochastic release time

Stochastic release time, i.e the the transport time, is an essential concept for the diffusion. For higher t, we will have higher displacement and higher diffusion. The equation is similar to x_f (eq. 2.14):

$$t = \frac{T_1 + T_2}{T_3 + T_4} \tag{2.22}$$

We define T_1, T_2, T_3, T_4 as follow:

$$\begin{aligned}
T_1(u) &= \int_0^{\pi} d\theta \sin\theta \int_0^{r_{nn}} dr 2\pi r^2 \int_{u-r\beta\cos\theta}^{r_{nn}+u-r(1+\beta\cos\theta)} d\epsilon \\
&\quad \times \frac{g(u)(1-F(v))}{v_0} \exp\left((1+\beta\cos\theta)r + \epsilon - u\right), \\
T_2(u) &= \int_0^{\pi} d\theta \sin\theta \int_0^{r_{nn}} dr 2\pi r^2 \int_{-\infty}^{u-r\beta\cos\theta} d\epsilon \frac{g(u)(1-F(v))}{v_0} \\
&\quad \times \exp((1+\beta\cos\theta)r) \\
T_3(u) &= \int_0^{\pi} d\theta \sin\theta \int_0^{r_{nn}} dr 2\pi r^2 \int_{u-r\beta\cos\theta}^{r_{nn}+u-r(1+\beta\cos\theta)} d\epsilon g(u)(1-F(v)), \\
T_4(u) &= \int_0^{\pi} d\theta \sin\theta \int_0^{r_{nn}} dr 2\pi r^2 \int_{-\infty}^{u-r\beta\cos\theta} d\epsilon g(u)(1-F(v))
\end{aligned} \tag{2.23}$$

Similarly to eq.2.13, $g(1-F)$ represents the emptiness of the arrival state. the exponential part can be summarized as: $exp(-r-u)$ and $\nu_0^{-1}exp(-r-u)$ represents the period of a jump. The born and the principle of the fraction is the same as for eq. 2.13. Here again, I_2 differs from I_1 at it doesn't take into account the energy part: the jump is downward in energy and doesn't need any tunneling effect regarding the energy.

From the fig. 2.10, we see that the time of a jump reaches 0 for high value. From what has been previously deduced, at high energy the jumps (which are rare), occurs solely on the energy level, and thus are practically instantaneous. For lower value, the states being farther away with lower energy, the particle will obviously takes more time to jump.

2.2.6 Diffusivity

From the definition of the diffusion, we have:

$$D = \frac{1}{2 \cdot n} \frac{d}{dt} \langle x^2(t) \rangle \tag{2.24}$$

- $\langle x(t) \rangle$: average displacement of a particle

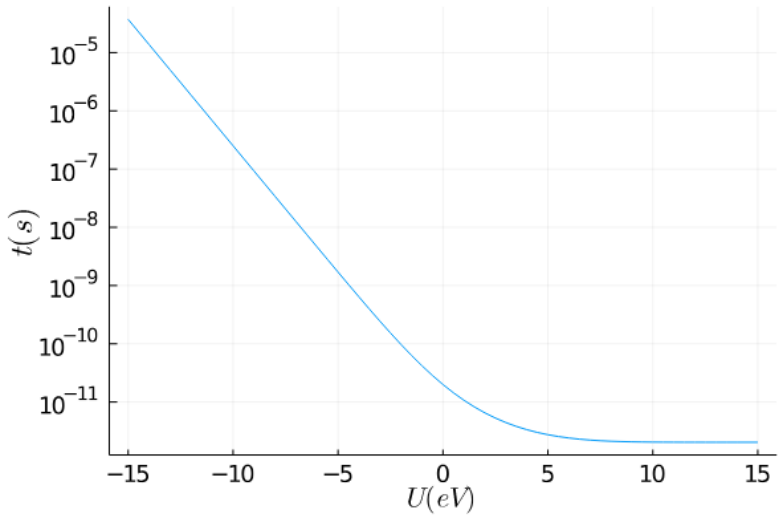

Figure 2.10: t dependence on the energy, $F = 5.3\,\mathrm{V\,cm^{-1}}$ (pentacene parameters appendix A)

- $n = 3$: dimension of the system, in our case

However, in presence of an electric field, a drift term appears in the equation 2.24:

$$D = \frac{1}{2 \cdot n} \frac{d}{dt} \langle (X(t) - \langle X(t) \rangle)^2 \rangle \tag{2.25}$$

$(X(t) - \langle X(t) \rangle$ is the drift of a certain displacement regarding the mean value. In a similar manner to eq. 2.18, we get:

$$\begin{aligned} D &= \frac{1}{2 \cdot n} \langle (X(t) - \langle X(t) \rangle)^2 \rangle \nu_0 e^{-r_{nn}} \\ D &= \frac{1}{6} \langle X(t)^2 - 2X(t)\langle X(t) \rangle - \langle X(t) \rangle^2 \rangle \nu_0 e^{-r_{nn}} \\ D &= \frac{1}{6} (\langle X(t)^2 \rangle - 2\langle X(t) \rangle \langle X(t) \rangle - \langle X(t) \rangle^2) \nu_0 e^{-r_{nn}} \\ D &= \frac{1}{6} (\langle X(t)^2 \rangle - \langle X(t) \rangle^2) \nu_0 e^{-r_{nn}} \end{aligned} \tag{2.26}$$

We define ΔX as the average displacement around the average position $\langle X \rangle$ in a way that: $X = \langle X \rangle + \Delta X$. ΔX is the pure randomness rising from the charge displacement. If we substitute X^2 by this new relation in eq. 2.26, we obtain:

$$
\begin{aligned}
D &= \frac{1}{6}(\langle[\langle X\rangle + \Delta X]^2\rangle - \langle X\rangle^2\rangle)\nu_0 e^{-r_{nn}} \\
D &= \frac{1}{6}(\langle\langle X\rangle^2 + 2\langle X\rangle\Delta X + \Delta X^2\rangle - \langle X\rangle^2)\nu_0 e^{-r_{nn}} \\
D &= \frac{1}{6}(2\langle X\rangle\Delta X + \Delta X^2\rangle)\nu_0 e^{-r_{nn}}
\end{aligned}
\tag{2.27}
$$

We propose the following expression for ΔX and $\langle X\rangle$:

$$
\begin{aligned}
\Delta X &= R_{nn} \\
\langle X\rangle &= X_F t\nu_0 e^{-r_{nn}}
\end{aligned}
\tag{2.28}
$$

ΔX is thus the distance non-influenced by the field and $\langle X\rangle$ is being influenced both by the field (through X_F) and by the time of transport. The quantity $t\nu_0 e^{-r_{nn}}$ model the number of jump made by a charge carrier.

At the end, we obtain the following formula:

$$
D = \frac{1}{6}(2X_F t\nu_0 e^{-r_{nn}} + R_{nn}^2)\nu_0 e^{-r_{nn}} \tag{2.29}
$$

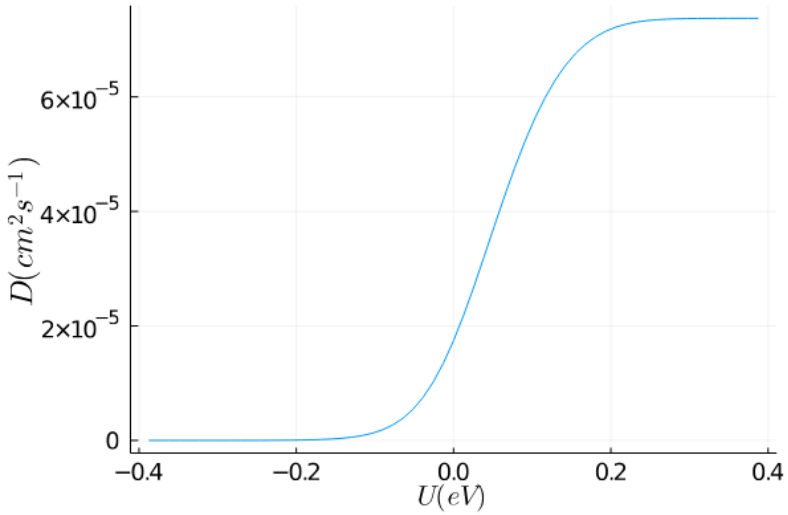

Figure 2.11: D dependence on the energy, $F = 5.3\,\mathrm{V\,cm^{-1}}$ (pentacene parameters appendix A)

From the figure 2.11, we see that for higher energy levels, D is higher. It is consistent with the precedent theory as with higher energy, particles have way

more possibility to move. In 2.29, we introduced ΔX which is the average deviation from the displacement and gives the constant value for higher energy as r_{nn} also takes into account the energy part of the jumps.

In the same fashion as with the mobility, the diffusivity is defined throughout the material by:

$$D = \frac{\int_{-\infty}^{+\infty} D(u)g(u)F(u)du}{\int_{-\infty}^{+\infty} g(u)F(u)du} \tag{2.30}$$

2.2.7 Einstein ratio

From the precedent value we computed, we can now define the einstein ratio as we will use it. Fist, the energy dependent one writes as:

$$EinsteinRatio(u) = \frac{D(u)}{\mu(u)} \tag{2.31}$$

However, as the relation is usually referred to its original equation (eq. 1.2), we will define η as:

$$\eta(u) = \frac{D(u)}{\mu(u)} \frac{q}{k_B T} \tag{2.32}$$

From the figure 2.12, we see that the einstein ratio attains a minimum for energy around the LUMO level. The value quickly rises for lower and higher energy level. For lower energy, it is admitted that traps cause higher η value. For greater energies, the quick decrease of the mobility due to the lack of spatial displacement as well as the constant D value due to the average variation of displacement ΔX, helps η ratio value to rise quickly.

2.2.8 Summary of some numerical value

To assess the viability of our model, we will perform some computation on the global values of μ, D, and η.

We performed a computation with $F = 4\,\mathrm{Vcm}^{-1}$, to respect the value measured in Xavier's thesis [11].

	$\mu(\mathrm{cm} \cdot \mathrm{V}^{-1} \cdot \mathrm{s}^{-1})$	$D(\mathrm{cm} \cdot \mathrm{s}^{-1})$	η
Values measured	2.15×10^{-5}	2.85×10^{-6}	5.1
Simulation	8.9×10^{-5}	5.45×10^{-6}	3.38

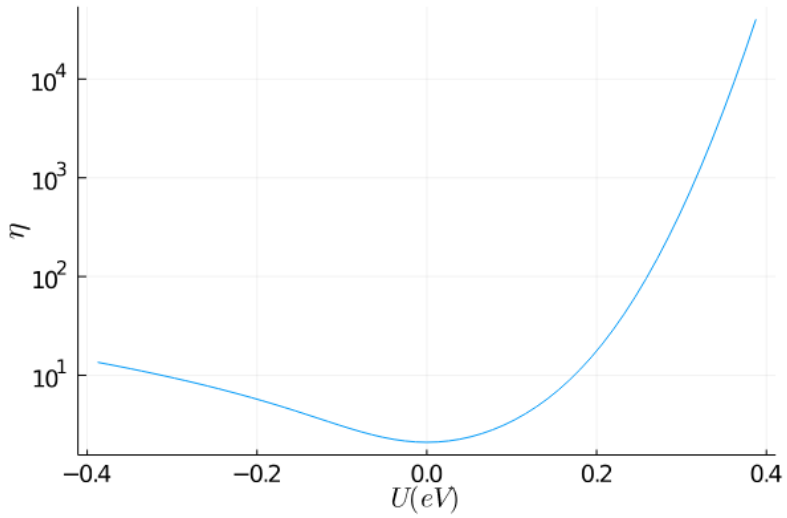

Figure 2.12: η dependence on the energy, $F = 5.3\,\mathrm{V\,cm^{-1}}$ (pentacene parameters appendix A)

The order of magnitude for the simulated values are comparable. However, the final simulated value η is a bit low compared to the real one measured. The overall mobility simulated is too high compared to the real one. It's due to a under-evaluated deep traps presence in the gaussian DOS. We also considered only energetic traps and spatial trap could be considered to reduce the overall mobility.

2.3 Parameters influence

Now that we have introduced all the parameters and equation for the electric part in our model, we can start to study the effect of different parameters on it.

2.3.1 Electric Field

The more obvious parameter to tweak is the field. It can easily be tuned by the bias voltage in a transistor for example.

For lower field ($\sim 1 \times 10^4\,\mathrm{V \cdot cm^{-1}}$), we observe a linearity for D (fig. 2.13). Regarding the mobility, we clearly see a quadratic dependence on the field (fig. 2.14). However, if we look closer at the numerical value, we can notice that for

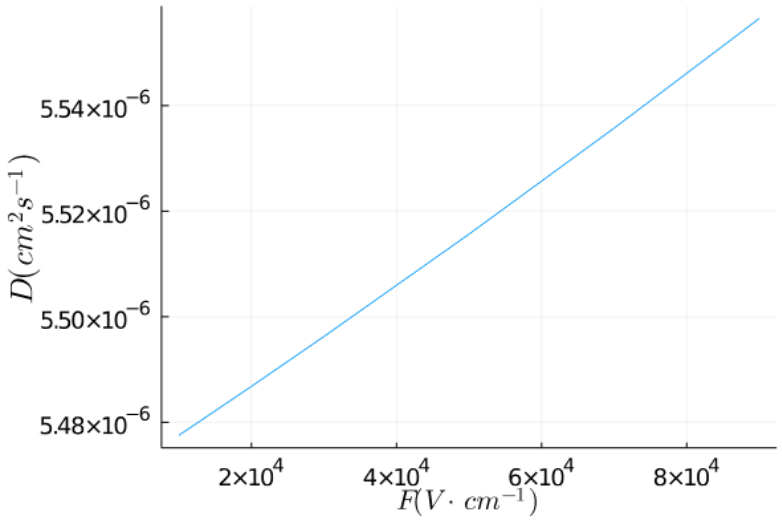

Figure 2.13: D dependence on low field (pentacene parameters appendix A)

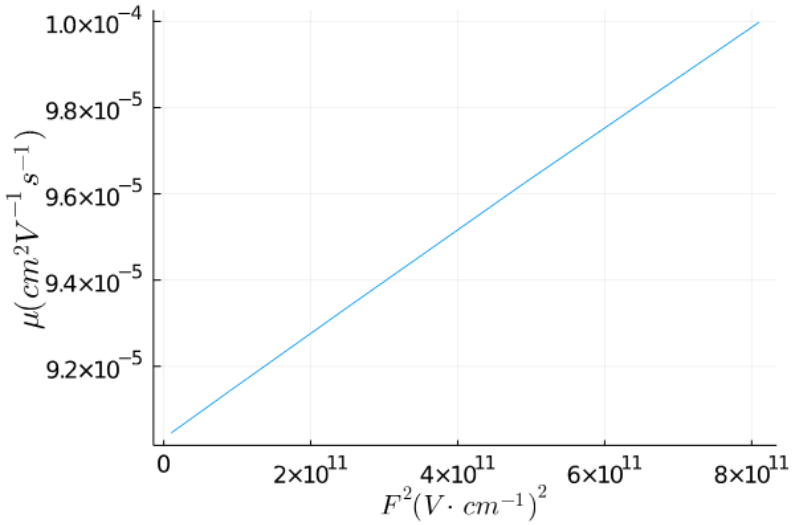

Figure 2.14: μ dependence on low field (pentacene parameters appendix A)

lower field the mobility is more or less constant. At the end, thanks to a constant mobility and a linear diffusivity regarding the field, the η value is also constant.

By increasing the field ($\sim 1 \times 10^5\,\mathrm{V \cdot cm^{-1}}$), we can observe a new behavior for the electric characteristics (fig. 2.16, 2.17, 2.18).

Indeed, the diffusivity D starts having quadratic behavior, as described in the

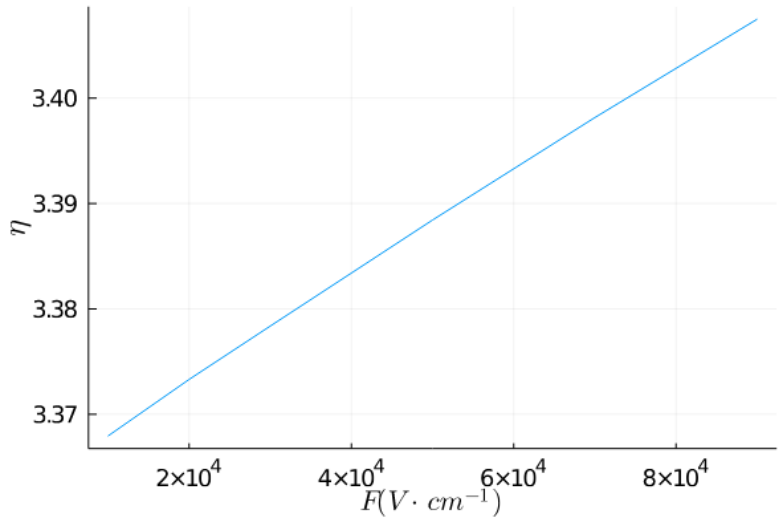

Figure 2.15: η dependence on low field (pentacene parameters appendix A)

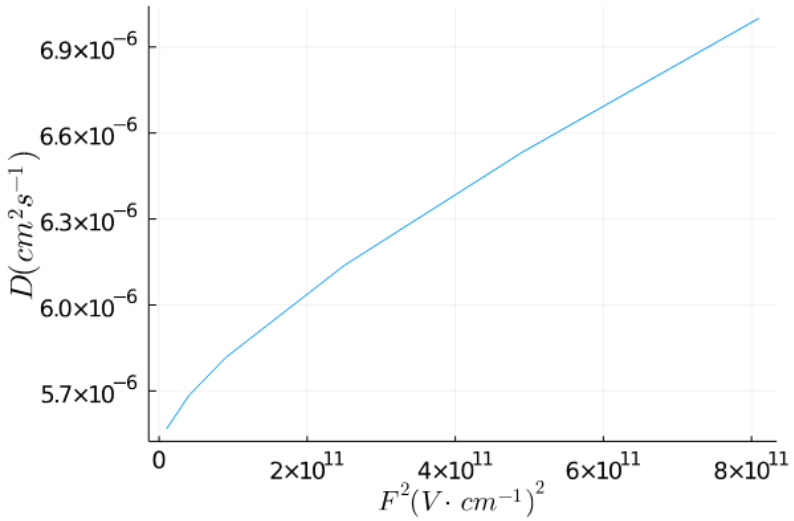

Figure 2.16: D dependence on high field (pentacene parameters appendix A)

paper [12]. While the mobility still has a quadratic behavior (fig. 2.17), it seems that the increase is greater for the μ value and that the einstein ratio η sees a local maximum for higher field (fig. 2.18).

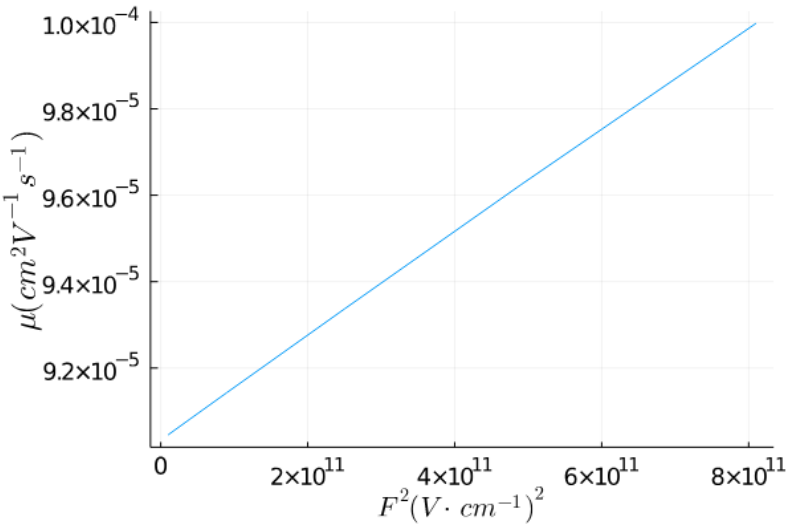

Figure 2.17: μ dependence on high field (pentacene parameters appendix A)

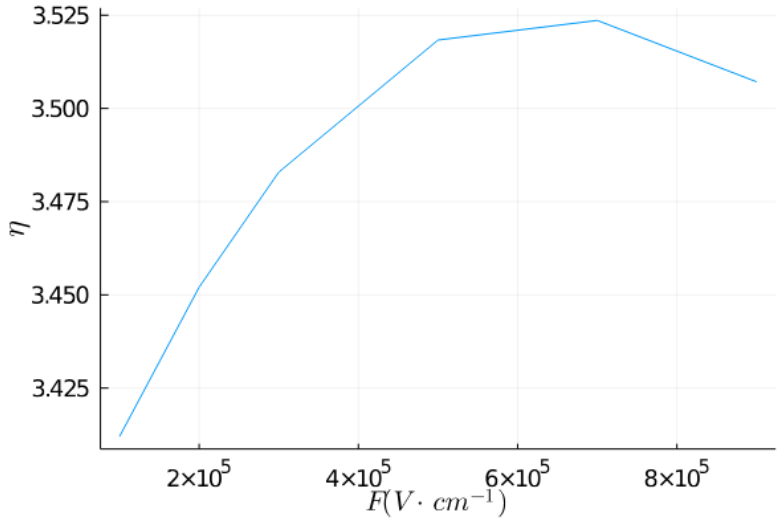

Figure 2.18: η dependence on high field (pentacene parameters appendix A)

2.3.2 Temperature

Chapter 3
Thermal properties

Thermal conduction is bore by both charge carriers and phonons however their behavior differs a lot. In the following part we will study both phonon and charge carrier transport regarding thermal characteristics.

3.1 Phonon transport

From the literature, it has been seen that for low frequencies phonon, a truncated gaussian DOS fits real devices behavior [23]. To simulate the truncated DOS, we will reduce the frequency of integration during the computation of k_p

$$g_p\left(E, \hbar\omega_\alpha\right) = \frac{1}{\sqrt{2\pi}} \frac{N_{i-e}}{\sigma_i} \exp\left(-\frac{\left(E - \hbar\omega_\alpha\right)^2}{2\sigma_i^2}\right) \tag{3.1}$$

The parameters of the DOS 3.1 are the same as for the pristine electric gaussian DOS. The material possesses the same features in term of phonon and charge carrier. Indeed, it has been observed [25] that the phonon displacement can be summed up by a series of jump between non propagating states. Besides, the usual vibration of a material is modeled by a discrete part [2] and a continuous part. We will here make the assumption that it can be simplified to a gaussian DOS.

3.1.1 Diffusivity

Acoustic phonons, the one that participate to the energy propagation, are deemed to be at low frequency and to quickly reach a plateau (fig. 3.1).

However, this behavior is a rough approximation and usually the phonon diffusion sees some discrete characteristics. But, in order to simplify and get an

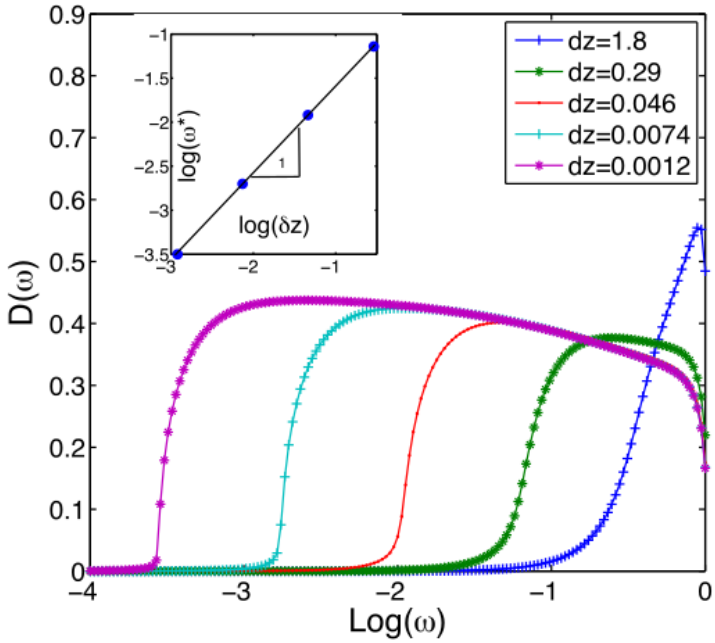

Figure 3.1: D dependence on the frequency ([29])

approximate result, we will assume such constant diffusion. To obtain an estimate of the value, we will base ourselves on the average diffusion for amorphous silicon:

$$D_p = 4.10 \times 10^{-6}\,\mathrm{m^2 s^{-1}} \tag{3.2}$$

3.1.2 Conduction

Usually, the thermal conduction is defined as [26]:

$$k_p = \frac{1}{V}\sum_i C_i(T) D_i \tag{3.3}$$

- i: summation over all the vibrational modes
- V: volume of the system
- Ci: spectral heat capacity
- D_i: thermal diffusivity

However, to simplify eq. 3.3, we will make the average over the frequencies [15]:

$$k_p = \int_{\omega_{min}}^{\omega_{max}} g'(\hbar\omega)C(\hbar\omega)D(\hbar\omega)d\omega \tag{3.4}$$

Please note that in equation 3.4, the DOS g' is given "in frequency": the unit is $\mathrm{Hz}^{-1}\mathrm{cm}^{-3}$. The spectral heat capacity is defined by:

$$\begin{aligned} C(\hbar\omega) &= \hbar\omega \frac{\partial d}{\partial T}\left[\left(e^{\frac{\hbar\omega}{k_B T}} - 1\right)^{-1}\right] \\ C(\hbar\omega) &= \hbar\omega \frac{e^{\frac{\hbar\omega}{k_B T}}}{\left(e^{\frac{\hbar\omega}{k_B T}} - 1\right)^2} \end{aligned} \tag{3.5}$$

In eq. 3.4, we defined a range for the integral through ω_{min} and ω_{max}. We first defined the spatial frequencies to be $400\,\mathrm{cm}^{-1}$ and $4000\,\mathrm{cm}^{-1}$ leading to frequencies of $1.2 \times 10^{13}\,\mathrm{Hz}$ and $1.2 \times 10^{14}\,\mathrm{Hz}$.

To make it work better with our model, we translated the frequency equation to the reduced energy one. First:

$$g'(\hbar\omega) = \hbar g(\hbar\omega) \tag{3.6}$$

By applying the change of variable $u = \frac{\hbar\omega}{k_B T}$:

$$k_p = k_B T \times \int_{u_{min}}^{u_{max}} g(u)C(u)D(u)du \tag{3.7}$$

3.2 Charge carrier transport

It has been demonstrated that charge carrier also participates to the heat conduction in semiconductors [4]. Such process arises because electron-hole pairs tend to be created at the hod end of the material and drift to the cold end, thus transmitting their energy.

It has been decided to use the same eq. 3.3 but with the charge carrier quantities D and g_e (eq. 2.29, 2.2). However, whereas for the phonons, only a small part of the frequencies were involved in the conduction process, for the electron we assume that all the frequencies participates to it. It also translate in the energy spectrum, thus:

$$k_e = k_B T \left(\int_{-\infty}^{0} g_e(u) C(u) D_e(u) du + times \int_{0}^{+\infty} g_e(u) C(u) D_e(u) du \right) \quad (3.8)$$

Of course, as explained in section 4.4.2, to enhance the performances, we used a reduced range to frame the energy levels where the charge carrier are.

Chapter 4
Julia implementation

4.1 Introduction

Julia is a recent open-source language (MIT) which has been developed specifically for scientific purposes. Syntax is also very similar to what can be done with Python, meaning that it's easy to read and write efficient code. Of course the syntax is also optimized for mathematics purpose, and the expressions are straightforwardly converted into the computer language. Even though it is a compiled language like Matlab, his use of REPL makes it quite easy to beta test code and run simple programs. The huge community involved around the language makes it easier to find useful package that are already optimized for fast computation in Julia. The support of other languages within the Julia language allows an even greater access to simple and user friendly tools: it is very easy to use the Python graphic renderer to plot and easily visualize data.

4.2 Performances

One key argument in choosing Julia over Matlab was its performances. According to the officials data (fig. 4.1), for this specific benchmark, Julia language reaches the performances of static-compiled languages such as C and is even better performing than Matlab.

4.3 Notebooks

The communication and presentation of data and code is a key part in making a scientific work. To help smoothing out the process, we intensively used Jupyter notebooks. They put in the same document programming language code, as well

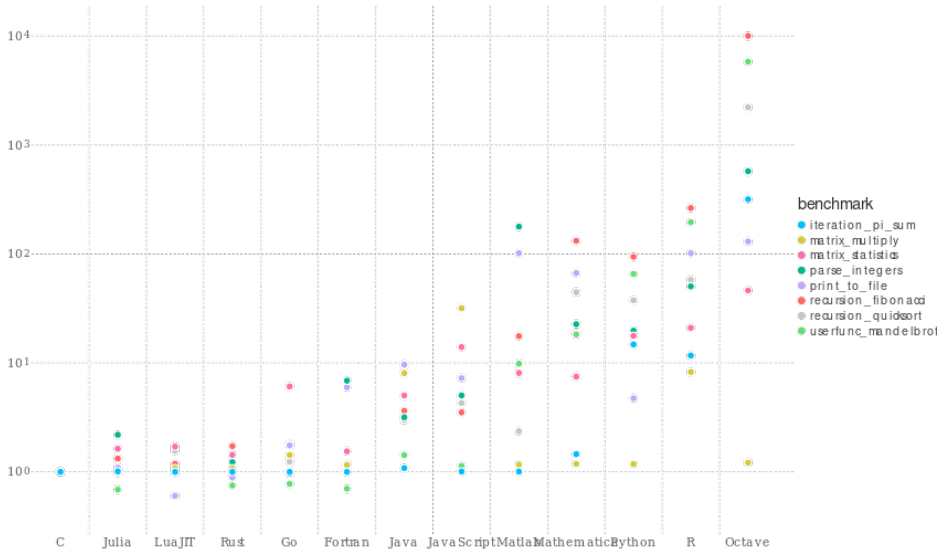

Figure 4.1: Julia benchmark

as plain text (rendered through markdown) to help clarify and improve the overall lisibility.

4.4 Code implementation

4.4.1 Reduced quantities

To help facilitate the comprehension of each function, reduced quantities for the energy and the spatial coordinates have been used as functions parameters.

```
function xf(semiconductor::Semiconductor, U::Real, T::Real,
    F::Real)::Float64
    R = Conduction.RnnVRH(semiconductor, U, T, F);

    return xf(semiconductor, R, U, T, F)
end
```

Typical functions for the diverse parameters are taking as parameters the semiconductor structure, energy, temperature and field intensity. Besides, we used extensively Julia's feature multiple dispatch to simplify and improve the

readability of the function. For example in code 4.4.1, the primal function xf computes an other function xf with different parameters. By doing so we can maintain a coherent environment for the function calls, the real computation being done by:

```
function xf(semiconductor::Semiconductor, Rnn::Real, U::Real,
    T::Real, F::Real)
    functionI = [I1, I2, I3, I4]
    resultI = Array{Float64}(undef, 4)

    for i in 1:4
        resultI[i] = functionI[i](U, T, semiconductor, Rnn, F)
    end

    return (resultI[1] + resultI[2]) / (resultI[3] + resultI[4])
end
```

4.4.2 Range of computation

For many quantities (mobility 2.18, ...) a global value requires an integral over all the possible energies of the form:

$$h = \frac{\int_{-\infty}^{+\infty} g(u)F(U)h(u)}{\int_{-\infty}^{+\infty} g(u)F(U)} \tag{4.1}$$

However, in the eq. 4.1, the range of integration doesn't allow a smooth computation in a reasonable amount of time: usually $h(u)$ function is complicated equation involving most of the time other integrals. To reduce the time of computation, one has to first reduce the range of integration. Thankfully to our model and the gaussian DOS, most of the charge carrier are trapped in a certain energy range (fig. 4.2). Such range has to be investigated for each change of material. For example with the pentacene (parameters fig 4.2), we see that for an energy of 0.4 eV, we have roughly 0.002 % of carrier (100 % being the maximum value for $U = \hbar\omega_\alpha$).

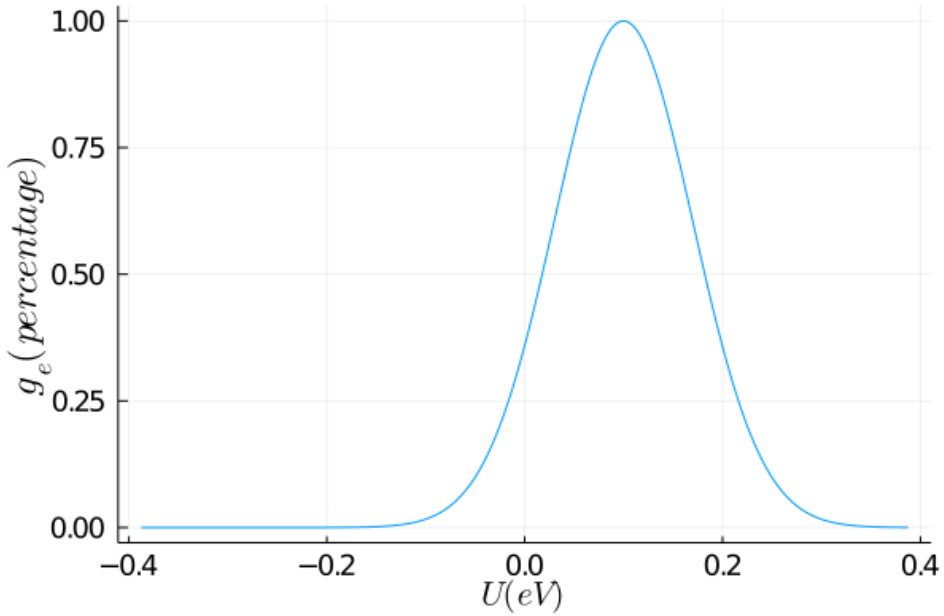

Figure 4.2: DOS compared to the maximum value

4.4.3 Integration in Julia

One of the key aspect of the modelisation that has been performed, was to perform easily and quickly complex integral over multiple dimension. The computation of 1D expression such as k_p (eq. 3.4) has been realized using QUADGK package:

```
kp(semiconductor, T) = k * T * quadgk(
    r -> DOSp(semiconductor, r, T) * C(r, T) * Dp(semiconductor, r,
        T),
    semiconductor.omega_min * hbar / (k * T),
    +Inf
)[1]
```

The multidimensional integrals have been computed using HCubature:

```
# Number of free state within a sphere of radius R
N(semiconductor::Semiconductor, U::Real, T::Real, R::Real)::Float64
    = (k * T) / (8 * semiconductor.alpha^3) * 2 * pi * hcubature(
    x -> DOS(semiconductor, var1(U, semiconductor.beta(T), R, x[1],
        x[2], x[3]), T) * (1 - F(semiconductor, var1(U,
```

```
    semiconductor.beta(T), R, x[1], x[2], x[3]), T)) * 1 / (1 -
    x[1])^2 * x[2]^2 * sin(x[3]),
[0, 0, 0],
[1, R, pi],
rtol=1e-6)[1]
```

However, concerning the multi-dimensional integrals, they can't be used as they were presented in the thesis. The parameters presented in the born have to be some constant and not depend on an other integral parameters.

Number of free states

The formula for the number of free state is taken from eq. 2.12 :

$$\mathcal{N}(u,T,\beta,\mathscr{R}) = \int_0^{\pi}\int_0^{\mathscr{R}}\int_{-\infty}^{\mathscr{R}+u-r(1+\beta\cos\theta)} g(v)\left[1-F(v)\right]\frac{kT}{8\alpha^3} \times 2\pi r^2\sin\theta\, dv\, dr\, d\theta \tag{4.2}$$

For the dv integrals, the superior born is defined by $\mathscr{R}+u-r(1+\beta\cos\theta)$, where θ and R' are already parameters for the first and second integral. In order to get rid of such born, we've made the change of variable:

$$v = \mathscr{R}+u-r(1+\beta\cos\theta) - \frac{t}{1-t} = a - \frac{t}{1-t} \tag{4.3}$$

It results in the change from eq. 4.2 to:

$$\mathcal{N}(u,T,\beta,\mathscr{R}) = \int_0^{\pi}\int_0^{\mathscr{R}}\int_0^{1} N\left(a-\frac{t}{1-t}\right)\left[1-F\left(a-\frac{t}{1-t}\right)\right]\frac{kT}{8\alpha^3} \times 2\pi r^2\sin\theta\frac{1}{(1-t)^2}\, dt\, dr\, d\theta \tag{4.4}$$

With this simple change of variable, the time of computation has been reduced from several minutes depending on the initial conditions, to a few seconds.

Real hopped distance

From the equation of the real hopped distance (eq. 2.14):

$$
\begin{aligned}
I_1 &= \int_0^{\pi} \int_{u-\overline{r_{nn}}\beta\cos\theta}^{u+\overline{r_{nn}}} N(v)\left[1-F(v)\right]\left[\frac{\overline{r_{nn}}-v+u}{1+\beta\cos\theta}\right]^3 \times \sin\theta\cos\theta dv d\theta \\
I_2 &= \int_0^{\pi} \int_{-\infty}^{u-\overline{r_{nn}}\beta\cos\theta} N(v)\left[1-F(v)\right]\overline{r_{nn}}^3\sin\theta\cos\theta dv d\theta \\
I_3 &= \int_0^{\pi} \int_{u-\overline{r_{nn}}\beta\cos\theta}^{u+\overline{r_{nn}}} N(v)\left[1-F(v)\right]\left[\frac{\overline{r_{nn}}-v+u}{1+\beta\cos\theta}\right]^2 \sin\theta dv d\theta \\
I_4 &= \int_0^{\pi} \int_{-\infty}^{u-\overline{r_{nn}}\beta\cos\theta} N(v)\left[1-F(v)\right]\overline{r_{nn}}^2\sin\theta dv d\theta
\end{aligned}
\tag{4.5}
$$

Similarly to the section 4.4.3, the area of integrals contain integrated variable θ. By the change of variable for I_1 and I_3:

$$
v = f_1(t) = \overline{\mathscr{R}_{nn}}\left[\frac{1+\beta\cos\theta}{t} - \beta\cos\theta\right] + u \tag{4.6}
$$

And by doing the change of variable for I_2 and I_4:

$$
v = f_2(t) = u - \overline{\mathscr{R}_{nn}}\beta\cos\theta - \frac{t}{1-t} \tag{4.7}
$$

We obtain the following formulas:

$$
\begin{aligned}
I_1 &= 0.5 * \overline{r_{nn}} \int_0^{\pi}\int_0^1 N\left(f_1(t)\right)\left[1-F\left(f_1(t)\right)\right]\frac{\left[\overline{r}_{nn}-f_1(t)+u\right]^3}{\left[1+\beta\cos\theta\right]^2}\sin(2\theta)dtd\theta \\
I_2 &= 0.5 * \overline{r_{nn}}^3 \int_0^{\pi}\int_0^1 N\left(f_2(t)\right)\left[1-F\left(f_2(t)\right)\right]\sin(2\theta)\frac{1}{(1-t)^2}dtd\theta \\
I_3 &= \overline{r_{nn}} \int_0^{\pi}\int_0^1 N\left(f_1(t)\right)\left[1-F\left(f_1(t)\right)\right]\frac{\left[\bar{r}_{nn}-f_1(t)+u\right]^2}{\left[1+\beta\cos\theta\right]}\sin(\theta)dtd\theta \\
I_4 &= \overline{r_{nn}}^2 \int_0^{\pi}\int_0^1 N\left(f_2(t)\right)\left[1-F\left(f_2(t)\right)\right]\sin(\theta)\frac{1}{(1-t)^2}dtd\theta
\end{aligned}
\tag{4.8}
$$

Stochastic time of release

From the equation of the stochastic time of release (eq. 2.22):

$$
\begin{aligned}
J_1(u) &= \int_0^{\pi} d\theta \sin\theta \int_0^{\overline{r_{nn}}} dr 2\pi r^2 \int_{u-r\beta\cos\theta}^{\overline{r_{nn}}+u-r(1+\beta\cos\theta)} du \\
&\quad \times \frac{\tau(u,u_F)}{v_0} \exp\left((1+\beta\cos\theta)r + u - u\right), \\
J_2(u) &= \int_0^{\pi} d\theta \sin\theta \int_0^{\overline{r_{nn}}} dr 2\pi r^2 \int_{-\infty}^{u-r\beta\cos\theta} du \frac{\tau(u,u_F)}{v_0} \\
&\quad \times \exp((1+\beta\cos\theta)r), \\
J_3(u) &= \int_0^{\pi} d\theta \sin\theta \int_0^{\overline{r_{nn}}} dr 2\pi r^2 \int_{u-r\beta\cos\theta}^{\overline{r_{nn}}+u-r(1+\beta\cos\theta)} du\tau(u,u_F), \\
J_4(u) &= \int_0^{\pi} d\theta \sin\theta \int_0^{\overline{r_{nn}}} dr 2\pi r^2 \int_{-\infty}^{u-r\beta\cos\theta} du\tau(u,\epsilon_F)
\end{aligned}
\tag{4.9}
$$

By doing the change of variable for J_1 and J_3:

$$
v = g_1(t) = t(\overline{r_{nn}} - r) + u + r\beta\cos\theta \tag{4.10}
$$

And by doing the change of variable for J_2 and J_4:

$$
g_2(t) = \frac{t}{t-1} + u - r\beta\cos\theta \tag{4.11}
$$

We obtain the following formulas:

$$
\begin{aligned}
I_1(u) &= \int_0^{\pi} d\theta \sin\theta \int_0^{\overline{r_{nn}}} dr 2\pi r^2 \int_0^1 dt \frac{\tau(g_1(t),u_F)}{v_0} \exp\left((1+\beta\cos\theta)r + g_1(t) - u\right) \\
I_2(u) &= \int_0^{\pi} d\theta \sin\theta \int_0^{\overline{r_{nn}}} dr 2\pi r^2 \int_0^1 dt \frac{\tau(g_2(t),u_F)}{v_0} \exp((1+\beta\cos\theta)) \\
I_3(u) &= \int_0^{\pi} d\theta \sin\theta \int_0^{\overline{r_{nn}}} dr 2\pi r^2 \int_0^1 dt\tau(g_1(t),u_F) \\
I_4(u) &= \int_0^{\pi} d\theta \sin\theta \int_0^{\overline{r_{nn}}} dr 2\pi r^2 \int_0^1 dt\tau(g_2(t),u_F)
\end{aligned}
\tag{4.12}
$$

4.5 Conclusion

Thanks to the possibilities of Julia and to numerous package, we could optimize the code to obtain a final computation of einstein ratio in the order of several

minutes/hours depending on the initial conditions.

Optimization is a key point to computational simulation as we need to get a result in a fair amount of time in order to work by iteration and tune our model to real data: we may want to fit a certain numerical value for instance.

References

[1] Apsley, N., and Hughes, H. P. Temperature-and field-dependence of hopping conduction in disordered systems. *The Philosophical Magazine: A Journal of Theoretical Experimental and Applied Physics 30*, 5 (1974), 963–972.

[2] Bakulin, A., Lovrincic, R., Yu, X., Selig, O., Bakker, H., Rezus, Y., Nayak, P., Fonari, A., Coropceanu, V., Brédas, J.-L., and Cahen, D. Mode-selective vibrational modulation of charge transport in organic electronic devices. *Nature Communications 6* (08 2015), 7880.

[3] Baranovskii, S., Faber, T., Hensel, F., Thomas, P., and Adriaenssens, G. Einstein's relationship for hopping electrons. *Journal of Non-Crystalline Solids 198-200* (1996), 214–217. Proceedings of the Sixteenth International Conference on Amorphous Semiconductors - Science and Technology.

[4] Berman, R. *Thermal Conduction in Solids*. OXFORD SCIENCE PUBLICATIONS. Clarendon Press, 1979.

[5] Brütting, W. Introduction to the physics of organic semiconductors. 1–14.

[6] Bässler, H. Charge transport in disordered organic photoconductors a monte carlo simulation study. *physica status solidi (b) 175*, 1 (1993), 15–56.

[7] Chiang, C. K., Fincher, C. R., Park, Y. W., Heeger, A. J., Shirakawa, H., Louis, E. J., Gau, S. C., and MacDiarmid, A. G. Electrical conductivity in doped polyacetylene. *Phys. Rev. Lett. 39* (Oct 1977), 1098–1101.

[8] Einstein, A. Über die von der molekularkinetischen Theorie der Wärme geforderte Bewegung von in ruhenden Flüssigkeiten suspendierten Teilchen. *Annalen der Physik 322*, 8 (Jan. 1905), 549–560.

[9] Einstein, A. Elementare betrachtungen über die thermische molekularbewegung in festen körpern [adp 35, 679 (1911)]. *Annalen der Physik 14*, S1 (2005), 408–424.

[10] Feldman, J. L., Kluge, M. D., Allen, P. B., and Wooten, F. Thermal conductivity and localization in glasses: Numerical study of a model of amorphous silicon. *Phys. Rev. B 48* (Nov 1993), 12589–12602.

[11] Kempa, X. *Study of the impact of Einstein relation enhancement on organic diodes in the case of variable range hopping.* PhD thesis, Keio University Graduate School of Science and Technology School of Integrated Design Engineering, 2020.

[12] Li, L., Lu, N., Liu, M., and Bässler, H. General einstein relation model in disordered organic semiconductors under quasiequilibrium. *Phys. Rev. B 90* (Dec 2014), 214107.

[13] Liu, C., Huang, K., Park, W.-T., Li, M., Yang, T., Liu, X., Liang, L., Minari, T., and Noh, Y.-Y. A unified understanding of charge transport in organic semiconductors: the importance of attenuated delocalization for the carriers. *Mater. Horiz. 4* (2017), 608–618.

[14] Lu, N., Li, L., Gao, N., and Liu, M. A unified description of thermal transport performance in disordered organic semiconductors. *Organic Electronics 41* (2017), 294–300.

[15] Lu, N., Li, L., Gao, N., and Liu, M. A unified description of thermal transport performance in disordered organic semiconductors. *Organic Electronics 41* (2017), 294–300.

[16] Miller, A., and Abrahams, E. Impurity conduction at low concentrations. *Phys. Rev. 120* (Nov 1960), 745–755.

[17] Minamiki, T., Minami, T., Chen, Y.-P., Mano, T., Takeda, Y., Fukuda, K., and Tokito, S. Flexible organic thin-film transistor immunosensor printed on a one-micron-thick film. *Communications Materials 2* (01 2021).

[18] Mitzi, D. B. Synthesis, structure, and properties of organic-inorganic perovskites and related materials. 1–121.

[19] Nenashev, A. V., Jansson, F., Baranovskii, S. D., Österbacka, R., Dvurechenskii, A. V., and Gebhard, F. Effect of electric field on diffusion in disordered materials. ii. two- and three-dimensional hopping transport. *Phys. Rev. B 81* (Mar 2010), 115204.

[20] Richert, R., Pautmeier, L., and Bässler, H. Diffusion and drift of charge carriers in a random potential: Deviation from einstein's law. *Phys. Rev. Lett. 63* (Jul 1989), 547–550.

[21] Roichman, Y., and Tessler, N. Generalized einstein relation for disordered semiconductors—implications for device performance. *Applied Physics Letters 80*, 11 (2002), 1948–1950.

[22] Sandanayaka, A. S. D., Matsushima, T., Bencheikh, F., Terakawa, S., Potscavage, W. J., Qin, C., Fujihara, T., Goushi, K., Ribierre, J.-C., and Adachi, C. Indication of current-injection lasing from an organic semiconductor. *Applied Physics Express 12*, 6 (may 2019), 061010.

[23] Schirmacher, W., Diezemann, G., and Ganter, C. Harmonic vibrational excitations in disordered solids and the "boson peak". *Phys. Rev. Lett. 81* (Jul 1998), 136–139.

[24] Shaw, J., and Seidler, P. Organic electronics: Introduction. *IBM Journal of Research and Development 45* (02 2001), 3 – 9.

[25] Shenogin, S., Bodapati, A., Keblinski, P., and McGaughey, A. J. H. Predicting the thermal conductivity of inorganic and polymeric glasses: The role of anharmonicity. *Journal of Applied Physics 105*, 3 (2009), 034906.

[26] Shenogin, S., Bodapati, A., Keblinski, P., and McGaughey, A. J. H. Predicting the thermal conductivity of inorganic and polymeric glasses: The role of anharmonicity. *Journal of Applied Physics 105*, 3 (2009), 034906.

[27] Shibata, M., Sakai, Y., and Yokoyama, D. Advantages and disadvantages of vacuum-deposited and spin-coated amorphous organic semiconductor films for organic light-emitting diodes. *J. Mater. Chem. C 3* (2015), 11178–11191.

[28] Stehr, V. *Prediction of charge and energy transport in organic crystals with quantum chemical protocols employing the hopping model*. PhD thesis, 06 2015.

[29] Wyart, M. Scaling of phononic transport with connectivity in amorphous solids. *EPL (Europhysics Letters) 89*, 6 (Mar 2010), 64001.

[30] Zhang, X., Dong, H., and Hu, W. Organic semiconductor single crystals for electronics and photonics. *Advanced Materials 30*, 44 (2018), 1801048.

Appendix

A Pentacene characteristics

The following values have been taken from the precedent work of Xavier [11] for pristine pentacene:

- $\alpha = 4.34 \times 10^7\,\mathrm{cm}^{-1}$
- $N_{i-E} = 3 \times 10^{21}\,\mathrm{cm}^{-3}$
- $\sigma = 0.071\,\mathrm{eV}$
- $E_F = -0.62\,\mathrm{eV}$
- $\nu_0 = 1 \times 10^{13}\,\mathrm{Hz}$